Welding in the World (2023) 67:2791–2802
https://doi.org/10.1007/s40194-023-01600-9

RESEARCH PAPER

Mechanical properties of MAG butt welded dissimilar structural steel joints with varying strength from grade S355 up to S960

Oliver Brätz[1] · Mareike von Arnim[2] · Stefan Eichler[3] · Andreas Gericke[1] · Jörg Hildebrand[3] · Jean Pierre Bergmann[3] · Ulrike Kuhlmann[2] · Knuth-Michael Henkel[1,4]

Received: 25 July 2023 / Accepted: 28 September 2023 / Published online: 14 October 2023

Abstract
Mixed connections made of normal-strength and high-strength structural steels allow for optimized material usage and production effort in applications where, as a result of different mechanical effects on materials of the same type, it would otherwise be necessary to adjust the plate thickness. Reduced material consumption and smaller weld geometries can thus generate ecological and economic advantages. When welding high-strength structural steels, however, significant softening can occur in the heat-affected zone, which can influence the load-carrying behavior of the overall joint. Since there are currently no appropriate standards for butt welds made of steels with different strengths up to S960, a separate design concept is required. In this paper, the weldability and load-carrying capacity of multilayer MAG welded butt joints designed as mixed connections of a normal-strength structural steel S355 and a high-strength structural steel in the range S690 to S960 are investigated. Extensive experimental investigations are carried out, in which other influencing variables such as the filler metal used, the heat input, the plate thickness, and the weld geometry are varied in order to identify their effects on the load-carrying capacity of the welded joints. Among other things, the results form the basis for an empirically based design model for mixed connections.

Keywords High-strength steel · Mixed connections · Joint design · Load-carrying capacity · Weldability · Impact toughness

1 Introduction

The use of high-performance weldable construction steels with increased strength allows the design of slender and filigree structures with long spans (see Fig. 1a). The high strength-to-weight ratio of these materials results in enormous advantages regarding the design weight, and therefore induce fewer material resource consumption and cost savings. Especially in the tensile area, cross-sectional dimensions can be reduced. As a secondary effect, the material requirements for the substructures can also be reduced, resulting in an improved life cycle assessment of the entire structure. In order to use structural steels with higher strength, commonly categorized according to their nominal yield strength as high-strength steels (HSS: $f_y = 460–690$ MPa) and ultra-high strength steels (UHSS: $f_y \geq 690–1100$ MPa), efficiently in structures, there may be a need for welded butt joints being mixed connections of normal-strength steel ($f_y = 355$ MPa) and HSS or UHSS. In bridge construction, cranes, offshore structures, or wind turbines, for example, the material load capacity can thus be adapted to the moment curve without having to adjust the plate thicknesses of the joint partner (cf. [1]). As a result, increased fabrication costs in the execution of thickness variations can be reduced, such as the mechanical preparation of the plates in the area of butt joints (see Fig. 1b). In addition, the reduced plate thicknesses result in a smaller weld seam

Recommended for publication by Commission XV - Design, Analysis, and Fabrication of Welded Structures

Oliver Brätz
oliver.braetz@igp.fraunhofer.de

1 Fraunhofer Institute for Large Structures in Production Engineering IGP, Albert-Einstein-Straße 30, 18059 Rostock, Germany

2 Institute of Structural Design, University of Stuttgart, Pfaffenwaldring 7, 70569 Stuttgart, Germany

3 Production Technology, Department of Mechanical Engineering, Technische Universität Ilmenau, Gustav-Kirchhoff-Platz 2, 98693 Ilmenau, Germany

4 Chair of Joining Technology, University of Rostock, Albert-Einstein-Straße 30, 18059 Rostock, Germany

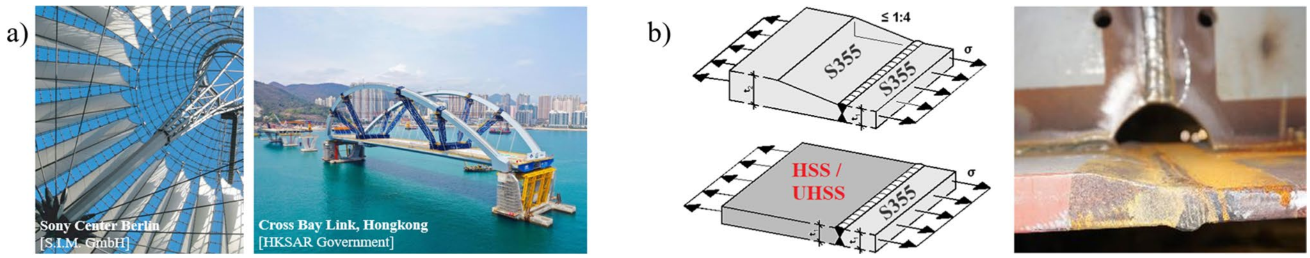

Fig. 1 **a** Application of high-strength steels, and **b** butt welds with individual load on joint partner executed with unequal thickness and chamfering of the thicker part vs. mixed connection of dissimilar steel strength with equal thickness

volume, so that enormous potential cost savings in production result from reduced welding times, filler materials, and possibly reduced preheating efforts. Notwithstanding, for certain fields, the lack of relevant experimental tests and limitations of the existing design standards due to uncertainty about the behavior of HSS/UHSS still hinder their wider applications in engineering practice [2–4]. Typical issues with regard to the metallurgical weldability of HSS/UHSS are, e.g., cold cracking in the heat-affected zone (HAZ) or weld metal, HAZ softening, hot cracking in weld metal, deterioration of toughness, and lack of ductility in HAZ [5–10].

The use of butt welds as mixed connections of steels with dissimilar strength is currently not clearly regulated by the European design code EN 1993-1-8 [11] for joint design in steel structures. Therefore, a research program funded by the German Federal Ministry for Economic Affairs and Climate Action was initiated in 2021, and comprehensive experimental as well as numerical studies were performed, see Acknowledgements. Different plate thicknesses ($t=3$, 10 and 20 mm), different groove types, different high-strength steel grades up to S960, different welding consumables (solid and metal cored wires with different filler metal strength), and heat inputs were used. With the results of the experimental and numerical investigations as well as further accompanying studies on the material properties, design rules for butt welds as mixed connections are being developed, which will in future influence the design rules in the second-generation of Eurocodes. In this paper, the weldability, i.e., the metallurgical behavior in particular, and the experimental results of investigation on the load-carrying capacity for mixed connections of construction steels with dissimilar strength and plate thicknesses of $t=10$ and 20 mm are presented.

The different welding behavior of dissimilar joined steels may cause a challenging metallurgy. For welding with filler metal, part of investigation was to predict the structure of the fusion zone and the risks associated with the different metal compositions. Moreover, welding of UHSS often involves consumables with lower strength, viz., undermatching filler materials [4, 12]. On one side, the selected welding parameters, i.e., heat input, effect the resulting weld metal microstructure, and thus need to be in a specific range to ensure certain material properties. On the other side, welding related HAZ formations differ for the dissimilar joint partner based on their composition and steel making process route and therefore must be considered, too [8]. For welding of S960MC with undermatching G46 filler metal, it was found that the resulting material properties differ significantly depending on the used welding process. In contrast to conventional gas metal arc welding (GMAW), joints realized by plasma welding reached the strength and toughness requirements of the base material. For GMAW, the use of a matching filler is necessary to achieve sufficient strength [12]. In contrast to typical normalized (N) low alloyed structural steels, when welding high-strength structural steels in quenched and tempered condition (QT) or as thermo-mechanically controlled process (TMCP or TM) steel, softening may occur within the heat-affected zone (HAZ) due to transformations and tempering effects, depending on the composition and the manufacturing process [13–15]. Depending on the extent of this soft zone with locally reduced strength, the load-carrying capacity of the entire joint can be negatively affected [6, 7, 16]. In some cases, a reduction of the load-carrying capacities by more than 15% has been observed compared to the ultimate tensile strength of the UHSS [16, 17]. Currently, no separate design checks are usually required for butt welds if the filler metal reaches at least the yield strength and ultimate tensile strength of the base material [11]. Accordingly, the general member check for the base material acc. to EN 1993-1-1 [18] is sufficient.

The current European standards for the design of steel structures (Eurocode 3) for joints EN 1993-1-8 [11, 19] and EN 1993–1–12 [20, 21] as extension up to steel grades S700 are insufficient for higher strength butt welds because the design is partly on the unsafe side [17]. These standards do not take into account the special metallurgical weldability of HSS/UHSS. For example, the formation of a soft zone in the HAZ is not covered. On the basis of experimental and numerical investigations [16, 22], a design concept has already been developed which allows an economical and safe design of high-strength butt welds. The concept applies to full penetration butt welds of steel grades greater than S460 and up to S700 using filler material with lower ('undermatching'), equal ('matching'), and higher ('overmatching') strength compared to the base material. The design concept has already been accepted by the responsible working group CEN TC250/SC 3/WG 8 for the final draft European standard FprEN 1993-1-8 [23].

Since the new edition prEN 1993-1-12 [24] is now to be extended for steel grades up to S960, tests were carried out on butt welds of similar steel grades S960QL as representative of a QT steel or S960MC as a TMCP steel [2]. For welding with matching filler materials, it was found that the new design model from FprEN 1993-1-8 leads to good agreements. However, for joints made with significantly undermatching G46 filler material, an adjustment of the model is necessary. With the results obtained, the design equation will then be extended up to S960. On welded joints of HSS up to S890 with unequal weld metal strength ('mismatch'), a significant influence on the failure behavior of the joint as a function of the mismatch ratio was found [17].

For mixed joints of normal-strength and high-strength steel up to S700, it is currently valid acc. to EN 1993-1-8 [11, 19] and EN 1993-1-12 [20, 21] for full penetration butt welds that the load-carrying capacity is equivalent to that of the weaker connected component. However, this has not yet been demonstrated for UHSS of the grade S960. In addition, the filler metal's specified strength ($R_{p0.2}$ and R_m), elongation at failure and Charpy V–notch (CVN) energy value should be equivalent to or better than that specified for the parent material [11]. Consequently, the filler metal must be oriented to the higher-strength steel. In this research project, see funding reference, extensive experimental and numerical investigations were carried out to analyze whether this procedure is necessary and whether the formation of a soft zone in mixed joints is relevant for the load-carrying and deformation capacity of the butt welds.

2 Experimental methodology

2.1 Material and sample welding

Various structural steel grades with different process routes (N, QT, and TMCP) and strengths were used. They correspond to the specified European standard technical delivery conditions for hot-rolled products made of structural steels (see Table 1). Both solid wire electrodes and metal cored wire electrode were used as consumables for metal active gas (MAG) welding using an Ar/CO_2 gas mixture (ISO 14175-M21-ArC-82/18) 15 l/min as shielding gas. The compositions of the used materials and the carbon equivalents representing their metallurgical weldability regarding welding-related hardening are listed in Table 2.

The weld samples were made fully mechanized by using a robot (Fig. 2a). Butt welds with a length of 600 mm were welded in flat position (ISO 6947-PA/1G acc. AWS). The width of the plates was 300 mm each (Fig. 2b). The rolling direction of the plates was oriented longitudinally to the weld. Either a single-V groove with an included angle of 60° and a 2-mm root face was one-side welded, or a 60° double-V groove with a 2-mm root face was double-side welded. The parameters for weld sample production are listed in Table 3 as average values obtained for the multi-pass welds. To investigate the influence of the heat input due to welding, different arc energies were selected. The 'low' arc energy was

Table 1 Used base materials and filler metals, specifications, and actual material properties

Material	Specification	Dimension	R_{eH} or $R_{p0.2}$ in MPa	R_m in MPa	A in %	KV_2 in J (at T)
S355J2+N, t10	EN 10025-2-S355J2+N (1.0577)	$t = 10$ mm	477	571	34	130 (−20 °C)
S355J2+N, t20		$t = 20$ mm	400	541	31	153 (−20 °C)
S690QL, t10	EN 10025-6-S690QL (1.8928)	$t = 10$ mm	859	887	14	165 (−40 °C)
S690QL, t20		$t = 20$ mm	851	883	17	170 (−40 °C)
S700MC, t10	EN 10149-2-S700MC (1.8974)	$t = 10$ mm	792	823	19	121 (−20 °C)
S960QL, t10	EN 10025-6-S960QL (1.8933)	$t = 10$ mm	1036	1077	11	27 (−40 °C)
S960QL, t20		$t = 20$ mm	1045	1074	14	138 (−40 °C)
G46	ISO 14341-A G 46 5 M21 4Si1	Ø1.2 mm	525	598	22	83 (−50 °C)
G69	ISO 16834-A G 69 6 M21 Mn4Ni1.5CrMo	Ø1.2 mm	761	806	18	81 (−60 °C)
G79	ISO 16834-A G 79 5 Mn4Ni1.5CrMo	Ø1.2 mm	889	940	17	57 (−50 °C)
G89	ISO 16834-A G 89 6 M21 Mn4Ni2CrMo	Ø1.2 mm	1040	1108	15	62 (−60 °C)
T69	ISO 18276-A T 69 6 Mn2NiMo M M21 2 H5	Ø1.2 mm	755	790	20	80 (−60 °C)
T89	ISO 18276-A T 89 4 Z M M21 3 H5	Ø1.2 mm	931	993	19	82 (−40 °C)

Table 2 Chemical composition of the used base materials and filler metals

Material	C wt.%	Si wt.%	Mn wt.%	Cr wt.%	Ni wt.%	Mo wt.%	Cu wt.%	P+S ppm	Al ppm	Ti ppm	B ppm	Nb ppm	V ppm	N ppm	*CET*[1)] in %
S355J2+N, t10	0.150	0.21	1.53	0.06	0.03	0.01	0.02	170	360	30	*n.a*	200	0	40	0.31
S355J2+N, t20	0.150	0.18	1.52	0.04	0.03	0.01	0.02	200	450	20	*n.a*	200	0	50	0.31
S690QL, t10	0.140	0.21	1.03	0.33	0.05	0.22	0.01	140	920	60	30	270	0	40	0.28
S690QL, t20	0.140	0.23	1.17	0.34	0.05	0.31	0.03	121	820	40	28	290	20	30	0.31
S700MC, t10	0.063	0.03	1.86	0.03	0.01	0.01	0.01	97	620	1350	2	530	70	*n.a*	0.25
S960QL, t10	0.167	0.29	1.39	0.28	0.12	0.52	0.10	100	270	20	28	260	20	50	0.38
S960QL, t20	0.165	0.28	1.08	0.19	0.04	0.52	0.02	120	*n.a*	180	14	10	10	*n.a*	0.34
G46	0.080	0.96	1.67	0.03	0.01	0.01	0.01	180	20	110	4	10	20	*n.a*	0.25
G69	0.080	0.56	1.65	0.24	1.58	0.47	0.03	170	30	640	10	40	30	*n.a*	0.34
G79	0.100	0.76	1.74	0.32	1.82	0.53	0.03	190	50	58	10	30	40	*n.a*	0.39
G89	0.110	0.83	1.78	0.37	2.24	0.57	0.01	170	30	750	1	30	30	*n.a*	0.42
T69	0.050	0.43	1.64	0.02	2.30	0.55	0.01	180	*n.a*	*n.a*	*n.a*	*n.a*	10	*n.a*	0.33
T89	0.090	0.51	1.29	0.55	2.80	0.82	*n.a*	220	*n.a*	*n.a*	*n.a*	*n.a*	*n.a*	*n.a*	0.40

[1]Carbon equivalent acc. ISO/TR 17671-2 – Method B: $CET = C + (Mn + Mo)/10 + (Cr + Cu)/20 + Ni/40$ in %

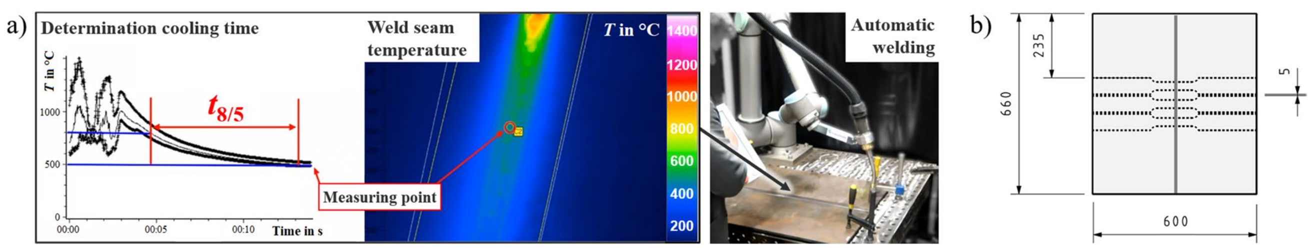

Fig. 2 Welding of specimens: **a** weld setup incl. cooling time determination, and **b** weld sample geometry and tensile test piece position (dimension in mm)

defined as welding processes that lead to a relatively short target cooling time of $t_{8/5} = 5$ s, describing the time interval for the cooling span from 800 to 500 °C of the weld metal. Corresponding to the high-strength steel involved, the 'high' arc energy corresponds to a defined target cooling time of $t_{8/5} = 8$ or 12 s, which represent the maximum processing recommendations specified by the steel manufacturer. The required lowest preheating temperatures were determined according to common concepts for the avoidance of hydrogen-assisted cold cracking based on the carbon equivalent *CET* of the filler metals and base metals, the geometry (form of weld and plate thickness), the heat input, and the expected maximum diffusible hydrogen contents in weld metal acc. to ISO/TR 17671-2 [25]. The present cooling times $t_{8/5}$ were determined by means of an infrared camera on the solidified weld beads (cf. [10]) (see Fig. 2a). Due to the different arc energies, the number of weld beads varied for the different samples to ensure full penetration joints. The samples were cooled in air or preheated again to ensure interpass temperatures equal to the preheating temperatures.

The test program comprises 36 weld samples with $t = 10$ mm and 24 weld samples with $t = 20$ mm. Three tensile test pieces were extracted per weld sample. Various combinations of base metal pairing (in each case normal strength S355J2 + N in combination with a high yield strength structural steel of grade S690QL/S700MC/S960QL), filler material (G46 as standard for S355 or a solid wire/tubular metal cored wire as matching filler metal with respect to the HSS/UHSS), heat input (high and low), and weld geometry (each as single-V and double-V groove) were investigated to cover a relevant range of applications.

2.2 Weld formation and hardness distribution

To investigate the metallurgical weldability and the local material condition, the welded joints were analyzed in transverse cross sections. The specimens were metallographically prepared and etched with alcoholic nitric acid, 3% Nital. Subsequently, microhardness mapping with 50-µm-grid was determined using an automatic tester (BAQ, UT 200) based on the ultrasonic contact impedance (UCI) method acc. to

Table 3 Mean welding parameter for sample manufacturing

Filler metal	Thickness t in mm	Joined HSS to S355J2+N	Heat input[1)]	Preheating T_P in °C	Arc type[2)]	Current I in A[3)]	Voltage U in V[3)]	Arc energy E in kJ/mm[4)]	Cooling time $t_{8/5}$ in s
Solid wire: G46, G69, G79 or G89	10	S690QL	Low (5)	25	p	214	25.0	0.82	5.7
		S700MC, S960QL		120	sc	207	22.6	0.61	5.2
		S960QL	High (8)	120	g	255	24.7	0.79	7.7
		S690QL	High (12)	25	s	307	28.2	1.21	11.7
		S700MC		120	s	272	28.3	0.97	13.0
	20	S690QL	Low (5)	170	p	208	25.3	0.81	4.3
		S960QL		150	g	247	25.0	0.83	5.2
		S690QL	High (8)	170	s	304	28.3	1.20	7.3
		S960QL		150	s	311	27.3	1.13	8.6
Metal cored wire: T89 or T69	10	S690QL,	Low (5)	25	s	298	25.9	1.03	6.6
		S960QL		120	g	187	29.8	0.74	5.4
		S960QL	High (8)	120	s	218	29.2	0.85	8.3
		S690QL	High (12)	25	s	325	26.7	1.19	9.9
	20	S690QL	Low (5)	170	s	290	25.9	1.00	5.4
		S960QL		150	g	232	29.4	0.91	5.1
		S690QL	High (8)	170	s	321	26.8	1.17	7.8
		S960QL		150	s	312	29.1	1.21	8.7

1) Target cooling time given in brackets as $t_{8/5}$ in s

2) Arc type/transfer mode: short circuit (sc), globular (g), spray (s) or pulse (p)

3) Mean value for standard arc welding, RMS value for pulse welding

4) Arc energy as heat input without consideration of an efficiency factor acc. to ISO/TR 18491

DIN 50159-1 [26]. A conversion of the results into the Vickers scale in HV 0.1 (UCI) was carried out. Validation of the UCI hardness measurement was previously made using reference measurements made with a conventional Vickers hardness tester (Struers, Durascan) (cf. [27]).

2.3 Mechanical weld testing

To investigate the load-carrying capacity, quasi-static transverse tensile tests until specimen break were carried out. Different test piece geometries were defined according to the plate thicknesses (see Fig. 3a). Three test specimens were taken from each weld samples in the central area of the weld length (see Fig. 2b). The weld reinforcement/convexity was removed by grinding. The tensile tests were performed on a 1-MN-testing machine with constant displacement-controlled testing speed. Specimens with plate thickness $t = 10$ mm were tested at 2 mm/min and specimens with plate thickness $t = 20$ mm were tested at 3 mm/min. For a more detailed analysis of the deformation behavior under loading, a spatially resolved strain measurement was performed using a high-resolution 3D camera system for

a)

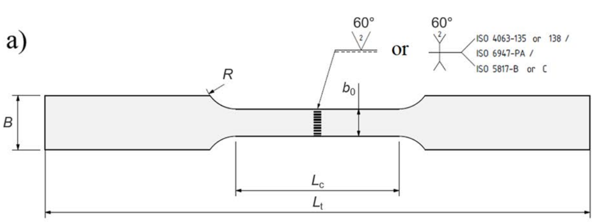

Thickness t in mm	Original width b_0 in mm	Radius R in mm	Parallel length L_c in mm	Total length L_t in mm	grip width B in mm
10	30	25	130	~ 600	60
20	30	35	180	~ 600	60

b)

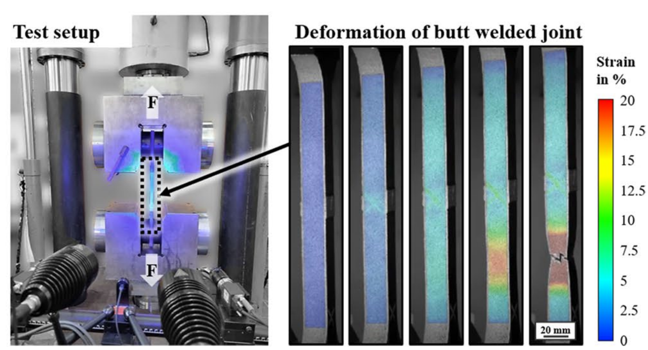

Fig. 3 Transverse tensile testing of the butt weld: **a** test piece geometry, and **b** test setup with optical strain measurement

full-field measurements (GOM, ARAMIS). Here, the distortion of a previously applied, irregular gray-scale pattern was recorded and evaluated (see Fig. 3b) with exemplary testing of a specimen with the same material pairing made of S960 [2].

In addition, circular cross-section test pieces (Ø10 mm, original gauge length $L_0 = 50$ mm) were taken from selected single-V weld samples $t = 20$ mm to characterize the strength and ductility of the weld metal. Charpy impact testing acc. to ISO 148–1 with standard V-notched test pieces ($10 \times 10 \times 55$ mm^3) transverse to weld was carried out to investigate the toughness properties in the welded joint. Since the direct comparison of CVN results is only of significance when made between test pieces of the same dimensions, only welds from $t = 20$ mm samples were tested to ensure extraction of standard size test pieces. The testing was performed by using a 450-J-pendulum (PSd 450, WPM Leipzig) equipped with a 2-mm striker. In accordance with a welding procedure qualification acc. to ISO 15614-1 [28], a set of three test pieces in the weld metal and in the HAZ each were tested. The specified impact properties required by base metal's technical delivery conditions must be fulfilled for the average value. One individual value may be below the specified value, provided that it is not less than 70% of that value. For joints of dissimilar metal, impact tests shall be carried out in the HAZ of both parent metal and the absorbed energy shall be in accordance with the parent material standard.

For the weld metal, the specimen location and notch orientation correspond to VWT 0/1 acc. to ISO 9016 [29], i.e., the notched face through plate thickness and position in the center line of the weld metal. The distance from the weld joint face side to the nearer face of the test specimen was 1 mm. For impact tests of the HAZ, specimens were taken with same notch geometry and at a 1-mm distance of the notch mid-point from the reference line, i.e., fusion line (VHT 1/1). The test temperatures were selected according to the specified impact properties of the base material with higher requirements.

3 Results and discussion

3.1 Weldability

For the assessment of weldability acc. to ISO/TR 581 [30], different aspects are to be evaluated together, i.e., metallurgical weldability as a material property, constructional weldability in virtue of its design, and operative weldability with respect to production conditions. The operative weldability of the examined processes is generally considered to be given due to the execution of common welding tasks (incl. joint preparation, preheating and execution of the welding work). The constructional weldability of the component under the intended operating loads and conditions must be taken into account in the design. The metallurgical weldability of the base materials and filler metals used was investigated for the welding procedures with different material pairings, heat inputs, and joint geometries regarding weld metallurgy, strength, and impact energy.

For all applied procedures, no metallurgical problems such as hot or cold cracking, or excessive embrittlement was found despite the sometimes very different base metal/filler metal combinations and the resulting weld metal composition (cf. [4]). The mechanical properties analyzed were strength by means of weld metal tensile tests and hardness distribution analysis in sectioned joint, and toughness by means of notched bar impact testing.

The hardness mapping across the joint area shows the transformation behavior and reveals the resulting inhomogeneous strength. The average hardness of the weld metal was found at a higher level for lower arc energies as a result of the accelerated cooling and the associated increasingly displacive phase transformation into microstructural constituents having high hardness. This is particularly evident in the cover pass region with slight reheating interaction, compare Fig. 4a and b, as well as e and f.

The average hardness of the G69 weld metal for the single-V groove ($t = 20$ mm) was about 340 HV 0.1 (UCI) for the lower arc energy of $E = 0.8$ kJ/mm ($t_{8/5} \approx 4$ s) and about 315 HV 0.1 (UCI) for $E = 1.19$ kJ/mm ($t_{8/5} \approx 7.5$ s). For the slower cooled G79 weld metal, there was an average hardness of about 310 HV 0.1 (UCI) for $E = 0.85$ kJ/mm ($t_{8/5} \approx 12$ s) and about 290 HV 0.1 (UCI) for $E = 1.1$ kJ/mm ($t_{8/5} \approx 18$ s). The comparison of the hardness of G89 weld metal of a single-V and double-V-groove weld does not reflect the influence of an increased proportion of reheated microstructure or the lower degree of dilution. At comparable heat input, this resulted in about 375 HV 0.1 (UCI) for the double-V-groove weld ($t_{8/5} \approx 8.4$ s) and 390 HV 0.1 (UCI) for the single-V-groove weld ($t_{8/5} \approx 7.5$ s).

At the side of S355J2 + N, a typical formation of the HAZ with characteristic regions depending on the temperature cycle was found, i.e., a considerably hardened area of up to about 350 HV 0.1 (UCI) in the coarse-grained region close to the fusion line (CGHAZ, $T_{max} \gg Ac_3$), a fine-grained/normalized region (FGHAZ, $T_{max} > Ac_3$) that was slightly influenced in terms of strength, as well as the intercritically heated region (ICHAZ, $Ac_1 < T_{max} \leq Ac_3$) and subcritical heated region (SCHAZ, $T_{max} < Ac_1$) that were slightly affected. With increased energy per unit length, the HAZ increased, but due to the associated longer cooling times, a microstructure with a tendency to a lower hardness level was formed, especially in the CGHAZ (cf. Figure 4a and b) on the right. The strength level of the normal-strength steel was not negatively affected by welding.

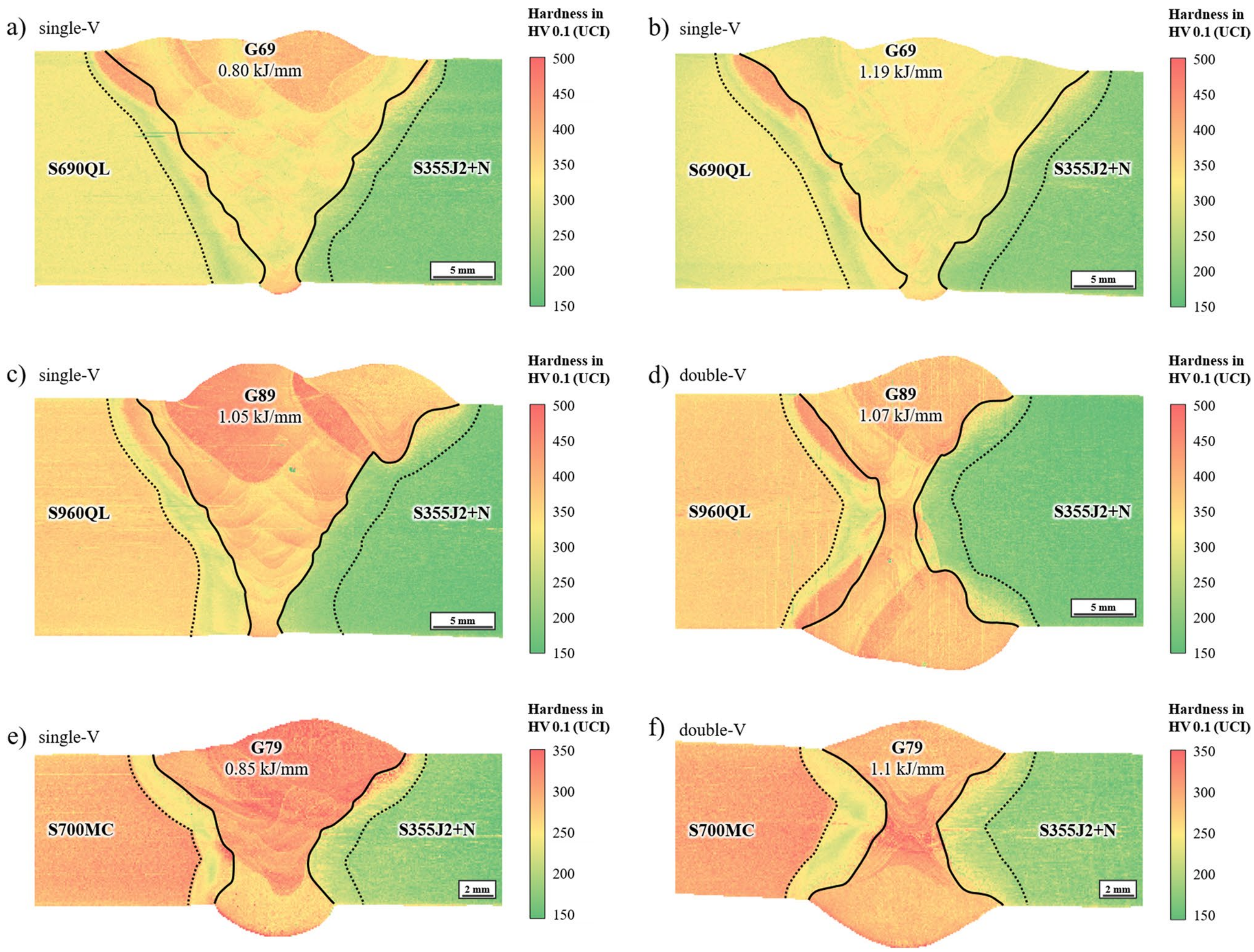

Fig. 4 Microhardness mapping in cross-section: **a** S690QL-S355J2+N joint ($t = 20$ mm) welded with G69 and low heat input compared to **b** welded with high heat input, **c** S960QL-S355J2+N joint ($t = 20$ mm) welded with G89 as single-V-groove weld compared to **d** double-V-groove weld, **e** S700MC-S355J2+N joint ($t = 10$ mm) welded with G79 as single-V-groove weld, and **f** as double-V-groove weld

The high-strength QT steels S690QL and S960QL exhibited a hardened region in the CGHAZ and FGHAZ in a range of approximately 410–430 HV 0.1 (UCI). In the ICHAZ and SCHAZ, a lower hardness level of approximately 250–290 HV 0.1 (UCI) was present which was below the hardness of the unaltered base material being about 310 and 360 HV 0.1 (UCI), respectively. Especially in the SCHAZ, tempering effects led to significant softening (see Fig. 4a to d left) [5, 15]. As a result of the multilayer welding procedure with locally superimposed temperature–time cycles, a complex microstructure resulted. The subcritically and intercritically reheated areas of the previous weld bead's HAZ were softened, too. Comparing the single-V and double-V-groove weld, a wider soft zone was present due to one-sided welding. In the case of welding on both sides, there was a larger proportion of the cover pass' HAZ over the plate thickness with as welded microstructure without reheating, so that an overall higher strength level was obtained in the joint, compare Fig. 4c and d, left. Based on the determined hardness mapping, it can be assumed that the permitted maximum hardness values within the scope of a procedure qualification acc. ISO 15614–1 [28] of 380 and 450 HV10 for N/TMCP steels and QT steels, respectively, can be met.

The weld metal strength was influenced by the different heat inputs or the associated resulting cooling times as well as the layer structure (see Fig. 5a). The G46 weld metal, which was welded with high arc energy containing a lower number of weld passes, exhibited higher strength. On the other hand, for the weld metal made of high-strength filler material G89 or T89, it was evident that a lower strength level was obtained with increasing cooling time. Only the G46 weld metal displayed a pronounced yield point in the stress–strain curve. The ductility of the high-strength weld metal was significantly lower than that of the G46. Moreover, high yield strength ratios of $R_{p0.2}/R_m > 0.92$ were found. All weld metal samples of the dissimilar joints met the

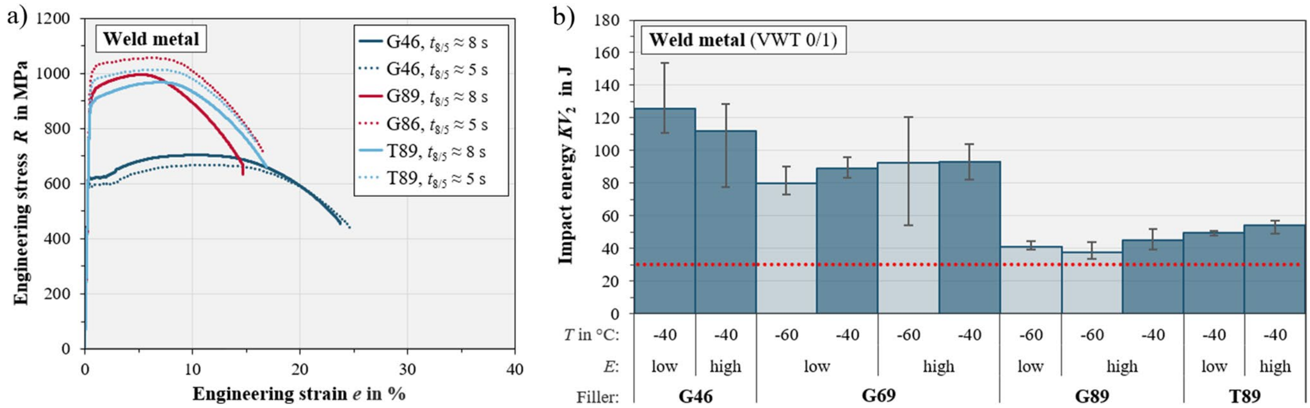

Fig. 5 Material properties of weld metal of $t = 20$ mm single-V-groove welds: **a** stress–strain curves, and **b** CVN impact energies for weld metal specimens of $t = 20$ mm butt welds compared with material requirements

requirements of their filler metal specifications. No relevant influence was found as a result of dilution with base metal of a significantly higher or lower strength class and differing composition [4].

The weld metal toughness properties of the single-V-groove welds $t = 20$ mm are represented by the impact energy values KV_2 for VWT 0/1 specimens in Fig. 5b). The error indicators refer in each case to the minimum and maximum values determined. The dark bars represent results from relevant test temperatures with regard to a procedure qualification. The pale bars show additional selected results from test temperatures in accordance with the filler material specification. All specimens met the minimum impact properties of 30 J at −40 °C specified for the base metals S690QL and S960QL [31]. As the strength of the weld metal increases, lower impact energy values were obtained. The highest impact energies of $KV_2 > 100$ J were found for G46 weld metal, and lowest of about 40 J for G89 weld metal, respectively, confirming earlier investigations [12]. The force–deflection curves recorded in the instrumented test procedure predominantly indicated a failure in the transition region with ductile content (Form E acc. to ISO 14556). Although the weld metal with higher strength reaches higher maximum forces, the ductile-to-brittle transition temperature of the HSS/UHSS are generally higher, so that increasingly lower impact energies were achieved at the same test temperature compared with the normal-strength steels.

All CVN specimens for HAZ testing (VHT 1/1) also achieved the required minimum impact properties of the respective base material standard, i.e., for S355J2+N at least 27 J at −20 °C and for high strength QT steels S690QL/S960QL at least 30 J at −40 °C [31], see Fig. 6.

Due to the inhomogeneous material state with varying proportions of HAZ and weld metal of the different filler metals in the ligament of the CVN test pieces, sometimes strong scattering occurs within a series. A tendential dependence on the groove geometry was not found. For the S355J2+N side, sufficiently high impact energies are achieved even when using high-strength filler metals. For the S960QL side, it can be seen that higher impact energy values

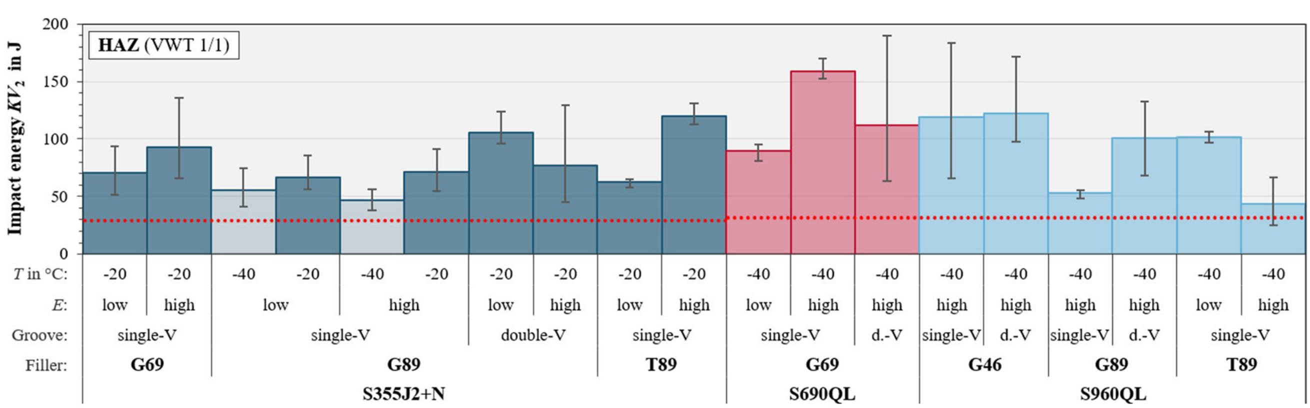

Fig. 6 CVN impact energies for HAZ specimens of $t = 20$ mm butt welds compared with material requirements

result for welds made with G46 filler metal. This is due to the higher toughness level of the undermatching G46 weld metal itself, since there is always a proportion of it present in the ligament. Generally, half-V-groove joints would allow to investigate separate HAZ subregions more accurate, but they were not considered in this study. Only single-V and double-V-groove joints were investigated due to their better operative weldability and higher relevance in manufacturing practice.

Based on the results of the destructive tests on the welded joints, a generally good weldability was found. In contrast to sophisticated rolling and heat treatment processes applied for base material manufacturing, the strength and toughness of the weld metal can only be achieved by solid solution and precipitation strengthening causing a higher concentration of refinement and hardening elements. Accordingly, metallurgical problems commonly result for these materials, i.e., sensitivity to excessive hardening, cold cracking, or solidification cracking [5, 9]. Nonetheless, neither the various mixtures of the different material compositions nor the different welding parameters and weld preparations were identified as critical in the range of variations applied. These findings are limited to the performed experimental work, i.e., welding procedures, and scope of testing. Especially for other processes with significantly different weld metallurgy, such as submerged arc or laser beam welding, the weldability might behave in a fundamentally different way.

3.2 Load-carrying capacity

The maximum load-carrying capacity σ_{max} of the welded joint was calculated as the maximum tension force in relation to the initial cross section S_0 at the point of failure in the parallel length area of the test piece. The determined load-carrying capacity is compared with the ultimate tensile strength R_m of the weaker joint partner, which always was the S355J2+N. The results for the specimens of plate thickness $t = 10$ mm are shown in Fig. 7. The error indicators refer in each case to the minimum and maximum values determined. The maximum nominal stresses determined for the $t = 10$ mm specimens ranged from 558 to 576 MPa. Taking into account the measurement uncertainties and typical scatter, this corresponds to the tensile strength of the S355J2+N. This matches with the typical failure behavior of the specimens.

Under tensile loading, no relevant deformation occurred in the weld metal or soft zone of the HSS's HAZ (see Fig. 8a). All specimens with $t = 10$ and 20 mm showed ductile failure in the unaltered base material (see representative fracture of a specimen in Fig. 8b). A local distribution of the deformation corresponding to the heterogeneous strengths in the weld joint region was not determined (cf. [17]).

The determined load-carrying capacities of the specimens with plate thickness $t = 20$ mm are shown in Fig. 9. The determined load capacities are all in the same range of 526–537 MPa, and thus also correspond to the tensile strength of the normal-strength steel. The soft zone within the HAZ of the high-strength steels is thus not considered relevant for the load-carrying capacity of the mixed joints with S355J2+N. It is not necessary to select the filler metal according to the higher strength steel connected. As expected, it is sufficient if the nominal strength (f_y and f_u) of the lower strength base metal is achieved.

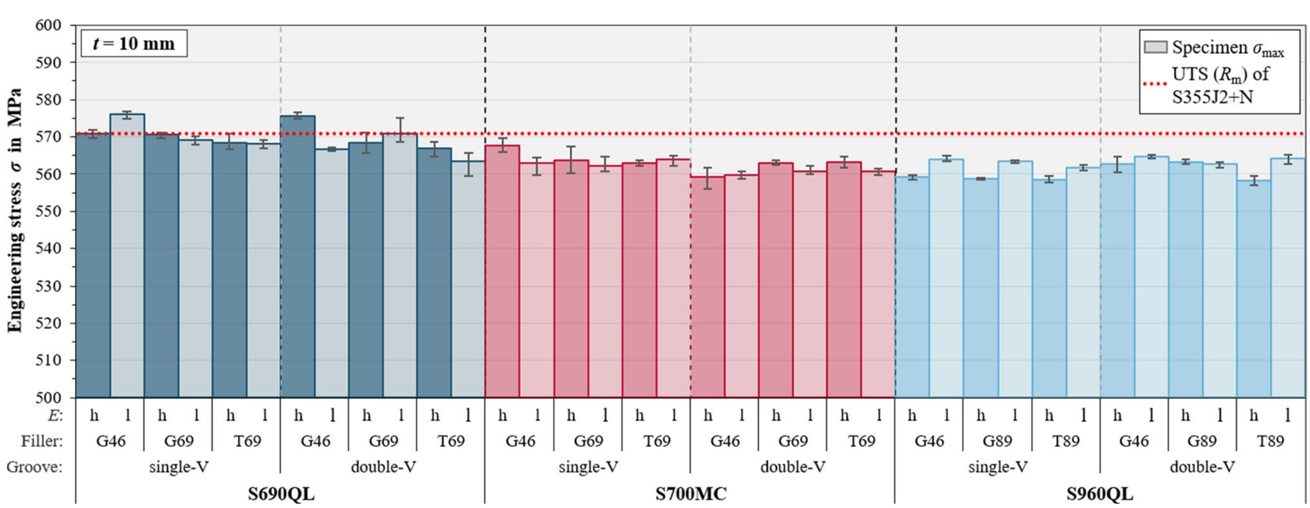

Fig. 7 Transverse load-carrying capacity of the dissimilar steel butt welds ($t = 10$ mm) compared with the ultimate tensile strength of the S355J2+N

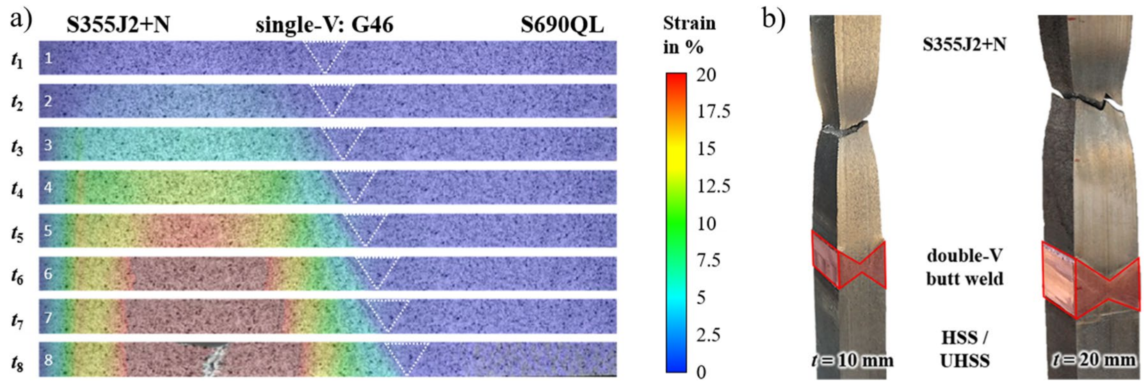

Fig. 8 Typical failure behavior of the dissimilar steel weld joints under transverse tension: **a** local strain distribution at different test times with increasing load levels, and **b** exemplary broken specimens with double-V-groove weld, $t = 10$ and 20 mm

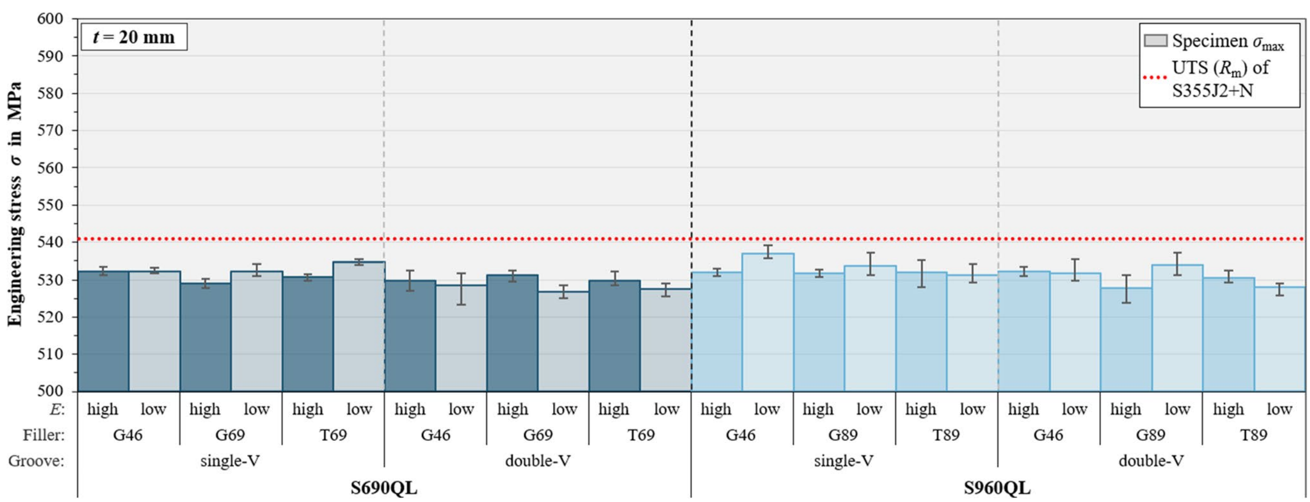

Fig. 9 Transverse load-carrying capacity of the dissimilar steel butt welds ($t = 20$ mm) compared with the S355J2 + N ultimate tensile strength

4 Conclusions

In this paper, multilayer MAG-welded mixed joints of the normal-strength steel S355J2+N in combination with an HSS/UHSS, viz., S690QL, S700MC, or S960QL, with a plate thicknesses of $t = 10$ and 20 mm, were investigated. The weldability was analyzed based on material property tests and the load-bearing behavior in the transverse tensile tests. Among other, the results provide the empirical basis for a new or extended design model for mixed joints up to S960. The following main conclusions are drawn:

a) The weldability of the investigated welding procedures as a combination of base material pairing, filler metal, heat input, and geometric joint configuration is given. The metallurgical weldability is suitable, and the material properties in the weld area required for weld procedure qualification acc. to ISO 15614-1 [28] have been proved for the samples with a thickness of $t = 20$ mm.

b) The HSS/UHSS underwent softening in the HAZ because of the temperature cycles during welding. The extent of this soft zone depended on the steel grade and the welding procedure, i.e., heat input and weld build-up. However, the average tensile strength in the soft zone of the high-strength steels S690QL, S700MC, and S960QL was always higher than the tensile strength of the unaltered normal-strength S355J2+N.

c) For all dissimilar steel butt welds as connections of S355J2+N and HSS/UHSS, the tensile strength of the normal-strength steel was always achieved in the transverse tensile test.

d) Failure occurred exclusively in the normal-strength steel. Also, no relevant strain was observed at the side with the higher strength joint partner. The soft zone formed in the

HAZ of the HSS/UHSS was identified as not relevant to the load-bearing behavior. Neither an influence on the load-carrying capacity nor on the failure behavior of the welded joint was found. No relevant deformation occurred in the soft zone.

e) There is no need to select a filler metal with a strength oriented to the high-strength joining partner to ensure the full load-carrying capacity of the mixed joint.

Acknowledgements The research project IGF 21412 BG/P 1507 'Effective design concepts for welded mixed connections in steel structures' from the Research Association for steel Application (FOSTA), Sohnstraße 65, 40237 Düsseldorf, Germany, is a sub-project of the FOSTA joint research program HOCHFEST and was supported by the Federal Ministry of Economic Affairs and Climate Action the German Federation of Industrial Research Associations (AiF) as part of the programme for promoting industrial cooperative research (IGF) on the basis of a decision by the German Bundestag.

Author contribution All authors contributed to the study conception and design. Sample manufacturing was contributed by O. B. and S. E. The experimental investigations and data analysis were carried out by O. B., M. v. A., and S. E. The first draft of the manuscript was written by O. B.. M. v. A. and S. E. commented on previous versions of the manuscript. K.-M. H., J. P. B., and U. K. helped supervise the project. J. P. B. and U. K. conceived the original idea. All authors discussed the results and commented on the manuscript.

Funding Open Access funding enabled and organized by Projekt DEAL.

Declarations

Conflict of interest The authors declare no competing interests.

References

1. Scharff R, Siems M (2014) Monopiles der nächsten Generation – Aspekte der Nachweisführung. Stahlbau 88(S2):2–9. https://doi.org/10.1002/stab.201430002
2. Brätz O, von Arnim M, Eichler S, Gericke A, Henkel K-M, Hildebrand J, Bergmann JP, Kuhlmann U (2023) Load-carrying capacity of MAG butt and fillet welded joints on high-strength structural steels of grade S960QL and S960MC. Ce/Papers 6(3–4):587–594. https://doi.org/10.1002/cepa.2478
3. Li D, Huang Z, Uy B, Thai H-T, Hou C (2019) Slenderness limits for fabricated S960 ultra-high-strength steel and composite columns. J Construct Steel Res 159:109–121. https://doi.org/10.1016/j.jcsr.2019.04.025
4. Mvola B, Kah P, Martikainen J, Suoranta R (2016) Dissimilar high-strength steels: fusion welded joints, mismatches, and challenges. Rev Adv Mater Sci 44(2):146–159
5. Tümer M, Schneider-Bröskamp C, Enzinger N (2022) Fusion welding of ultra-high strength structural steels — a review. J Manuf Proces 82:203–229. https://doi.org/10.1016/j.jmapro.2022.07.049
6. Maurer W, Ernst W, Rauch R, Vallant R, Enzinger N (2015) Evaluation of the factors influencing the strength of HSLA steel weld joint with softened HAZ. Weld World 59:809–822. https://doi.org/10.1007/s40194-015-0262-z
7. Amraei M, Ahola A, Afkhami S, Björk T, Heidarpour A, Zhao X-L (2019) Effects of heat input on the mechanical properties of butt-welded high and ultra-high strength steels. Eng Struct 198:109460. https://doi.org/10.1016/j.engstruct.2019.109460
8. Bayock FN, Kah P, Mvola B, Layus P (2019) Effect of heat input and undermatched filler wire on the microstructure and mechanical properties of dissimilar S700MC/S960QC high-strength steels. Metals 9(8):883. https://doi.org/10.3390/met9080883
9. Chen Z, Xiong Y, Qiu H, Lin G, Li Z (2018) Stress intensity factor-based prediction of solidification crack growth during welding of high strength steel. J Mater Process Technol 252:270–278. https://doi.org/10.1016/j.jmatprotec.2017.09.031
10. Zhang Y, Xiao J, Liu W, Zhao A (2021) Effect of welding peak temperature on microstructure and impact toughness of heat-affected zone of Q690 high strength bridge steel. Mater 14(11):2981. https://doi.org/10.3390/ma14112981
11. EN 1993-1-8:2005+AC:2009 (2009) Eurocode 3: Design of steel structures - Part 1-8: Design of joints. CEN, Brussels
12. Schneider C, Ernst W, Schnitzer R, Staufer H, Vallan R, Enzinger N (2018) Welding of S960MC with undermatching filler material. Weld World 62:801–809. https://doi.org/10.1007/s40194-018-0570-1
13. Cai W-Y, Wang Y-B, Li G-Q, Stroetmann R (2022) Comparative study on strength of TMCP and QT high-strength steel butt-welded joints. J Construct Steel Res 197:107447. https://doi.org/10.1016/j.jcsr.2022.107447
14. Zhang L, Kannengiesser T (2016) HAZ softening in Nb-, Ti- and Ti + V-bearing quenched and tempered steel welds. Weld World 60:177–184. https://doi.org/10.1007/s40194-016-0299-7
15. Afkhami S, Javaheri V, Amraei M, Skriko T, Piili H, Zhao X-L, Björk T (2022) Thermomechanical simulation of the heat-affected zones in welded ultra-high strength steels: Microstructure and mechanical properties. Mater Des 213:110336. https://doi.org/10.1016/j.matdes.2021.110336
16. Bergmann JP, Hildebrand J, Kuhlmann U, Spiegler J, Keitel S, Mückenheim U (2020) Tragfähigkeit von Stumpfnähten höherfester Stähle im Stahlbau, Research report IGF 19470 B. DVS Media, Düsseldorf
17. Ran M-M, Sun F-F, Li G-Q, Kanvinde A, Wang Y-B, Xiao RY (2019) Experimental study on the behaviour of mismatched butt welded joints of high strength steel. J Construct Steel Res 153:196–208. https://doi.org/10.1016/j.jcsr.2018.10.003
18. EN 1993-1-1:2005+AC:2009 (2009) Eurocode 3: Design of steel structures - Part 1-1: General rules and rules for buildings. CEN, Brussels
19. DIN EN 1993-1-8/NA:2020-11 (2020) National Annex - Nationally determined parameters - Eurocode 3: Design of steel structures - Part 1-8: Design of joints. DIN, Berlin
20. EN 1993-1-12:2007+AC:2009 (2009) Eurocode 3: Design of steel structures - Part 1-12: Additional rules for the extension of EN 1993 up to steel grades S700. CEN, Brussels
21. DIN EN 1993-1-12/NA:2011-08 (2011) National Annex - Nationally determined parameters - Eurocode 3: Design of steel

structures - Part 1-12: Additional rules for the extension of EN 1993 up to steel grades S700. DIN, Berlin
22. Spiegler J (2022) Tragfähigkeit von Kehlnaht- und Stumpfnaht-verbindungen höherfester Baustähle. Dissertation, University of Stuttgart, Institut für Konstruktion und Entwurf, Mitteilung No. 2022-2. https://doi.org/10.18419/opus-12207
23. FprEN 1993-1-8:2023 (2023) Eurocode 3: Design of steel structures - Part 1-8: Joints. Formal vote version. CEN/TC 250, Brussels
24. CEN/TC 250/SC 3/WG 12 N118 (2021) prEN 1993-1-12: Eurocode 3 - Design of steel structures - Part 1-12: Additional rules for steel grades up to S960. Working Draft (unpublished). CEN, Brussels
25. ISO/TR 17671-2 (2002) Welding - Recommendations for welding of metallic materials - Part 2: Arc welding of ferritic steels. ISO, Geneva
26. DIN 50159-1 (2022) Metallic materials - Hardness testing with the UCI method - Part 1: Test method. DIN, Berlin
27. von Arnim M, Eichler S, Brätz O, Hildebrand J, Gericke A, Kuhlmann U, Bergmann JP, Flügge W (2022) Effiziente Nach-weiskonzepte für geschweißte Mischverbindungen im Stahlbau. Stahlbau 91(10):660–670. https://doi.org/10.1002/stab.202200046
28. EN ISO 15614-1:2017+A1:2019 (2019) Specification and qualification of welding procedures for metallic materials - Welding procedure test - Part 1: Arc and gas welding of steels and arc welding of nickel and nickel alloys. CEN, Brussels
29. ISO 9016 (2022) Destructive tests on welds in metallic materials - Impact tests - Test specimen location, notch orientation and examination. ISO, Vernier
30. ISO/TR 581:2005 (2005) Weldability - Metallic materials - General principles. ISO, Geneva
31. EN 10025-6:2019+A1:2022 (2022) Hot rolled products of structural steels - Part 6: Technical delivery conditions for flat products of high yield strength structural steels in the quenched and tempered condition. CEN, Brussels